

# Non-enzymatic glucose detection using nitrogen-doped diamond-like carbon electrodes modified with gold nanoclusters\*

Aiping Liu<sup>1,2</sup>, Erjia Liu<sup>1,‡</sup>, Guocheng Yang<sup>1</sup>, Nay Win Khun<sup>1</sup>, and Wenguang Ma<sup>1</sup>

<sup>1</sup>School of Mechanical and Aerospace Engineering, Nanyang Technological University, 50 Nanyang Avenue, Singapore 639798, Singapore; <sup>2</sup>Department of Physics, Center for Optoelectronics Materials and Devices, Zhejiang Sci-Tech University, Xiasha College Park, Hangzhou 310018, China

**Abstract:** Highly sensitive electrochemical electrodes for glucose detection were developed by using Au nanoclusters (NCs) to modify nitrogen-doped diamond-like carbon thin films (DLC:N/Au). The DLC:N/Au electrodes were prepared with a filtered cathodic vacuum arc process followed by electrodeposition and characterized by X-ray photoelectron spectroscopy, Raman spectroscopy, and scanning electron microscopy. The size of the Au NCs covered by Au oxide ranged between 10 and 70 nm with a density of  $10^8$ – $10^9$  clusters per  $\text{cm}^2$ . Glucose oxidation at the DLC:N/Au electrodes started from about  $-0.5$  V due to the high catalytic activities of the Au NCs in NaOH solutions, and the catalytic ability of the electrodes depended on the amount of Au NCs deposited on the electrode surfaces. A linear detection range of glucose with the DLC:N/Au electrodes was identified from about 0.25 to 30 mM (covering blood glucose levels in diabetic patients) with a detection limit of 60  $\mu\text{M}$ . The experimental results showed that the non-enzymatic glucose sensors based on the DLC:N/Au electrodes had high sensitivity and good reproducibility and stability.

**Keywords:** catalytic activity; glucose detection; gold nanoclusters; nitrogen-doped diamond-like carbon thin film.

## INTRODUCTION

Glucose detection and determination are of great importance in the fields of biological, environmental, clinical, and food analyses [1,2]. Glucose sensors are convenient in monitoring the concentration of glucose under actual conditions including extreme conditions inside the human body, which requires the materials and configurations of the sensors to be chemically stable and biocompatible. Metal and noble metal electrodes with high electrocatalytic activities, such as Ni, Cu, Pt, and Au, have been widely used to oxidize carbohydrates in liquid chromatography and capillary electrophoresis [3–6]. However, the oxidized products may be easily adsorbed onto the metal electrode surfaces, causing a decrease in activity and poisoning of the electrodes [7]. Furthermore, the poor biocompatibility of metal electrodes also restricts their applications in *in vivo* detection. Carbon materials with excellent biocompatibility

---

\*Paper based on a presentation at the 5<sup>th</sup> International Symposium on Novel Materials and Their Synthesis (NMS-V) and the 19<sup>th</sup> International Symposium on Fine Chemistry and Functional Polymers (FCFP-XIX), 18–22 October 2009, Shanghai, China. Other presentations are published in this issue, pp. 1975–2229.

<sup>‡</sup>Corresponding author: Tel.: +65 67905504; Fax: +65 67924062; E-mail: mejliu@ntu.edu.sg

are regarded superior to noble metals due to their low cost, wide potential window, and relative inertness in both aqueous and nonaqueous media [8–13]. Glucose detection using different carbon electrodes has been widely reported in the past few years [14–18]. For example, Zhang et al. developed an amperometric glucose biosensor based on immobilization of glucose oxidase in a nonconducting poly(*o*-aminophenol) film on a platinized glassy carbon electrode [14]. Wang et al. investigated the covalent immobilization of redox enzymes onto electrically conductive nanocrystalline diamond thin films to detect glucose [15]. Lin and co-workers developed glucose biosensors based on carbon nanotubes and glucose oxidase covalently bonded nanoelectrode ensembles for the selective detection of glucose [17]. However, most of the studies on this subject involved glucose oxidase. The stability and activity of enzyme in these sensors, which are affected by temperature, pH, and oxygen, etc., determine and control the performances of glucose sensors. Direct oxidation of glucose at an enzyme-free electrode was therefore proposed to improve the stability of glucose sensors used in different environments [19,20].

Diamond-like carbon (DLC) thin films composed of  $sp^2$  and  $sp^3$  hybridized carbon show relatively high hardness, excellent biocompatibility, and chemical inertness, and high corrosion resistance similar to diamond films [13]. By introducing impurity elements, such as N, P, and Ni, the doped DLC films can possess sufficient conductivity (electrical resistivity:  $1\text{--}10^4 \Omega\cdot\text{cm}$ ) for electrochemistry, low double layer capacitance, large potential window, low background current, high stability in challenging environments, and comparative resistance to deactivation by fouling [8,11,12,21–24], and thus are regarded appropriate for glucose detection. However, similar to boron-doped diamond (BDD) film electrodes, the electrocatalytic activity of doped DLC electrodes for glucose oxidation is still limited [19]. Metallic nanoparticles (NPs) or nanoclusters (NCs) loaded on an inert electrode surface represent obvious differences in physical and chemical properties from both substrate materials and isolated bulk metals, and may drastically increase the catalytic activity and sensitivity of the electrodes, resulting in the enhancement of the performances of biosensors [25–27]. Large surface areas and good electronic properties of dispersive metallic particles, such as Cu, Au, Pt, and Ni, can accumulate charges and improve electrochemical response of carbon electrodes in electrochemical glucose sensors [28–32]. For example, Watanabe et al. reported the oxidation behavior of glucose on a metal-implanted BDD electrode [28]. Mena and co-workers designed Au NP-modified glassy carbon electrodes by electrodeposition to detect glucose and analyze kinetic parameters of glucose sensors [29]. Hrapovic et al. prepared Pt NPs with 2–3 nm in diameter in combination with single-wall carbon nanotubes for fabricating electrochemical glucose sensors [30]. However, to our knowledge, there were fewer reports on glucose oxidation on metallic NPs- or NCs-modified conductive DLC electrodes.

In this study, nitrogen-doped DLC (DLC:N) thin films modified with Au NCs (DLC:N/Au) were fabricated, and the resulting DLC:N/Au electrodes were characterized by X-ray photoelectron spectroscopy (XPS), Raman spectroscopy, and scanning electron microscopy (SEM). The capability of non-enzymatic DLC:N/Au films as an analytical electrode for glucose detection was investigated by voltammetric measurement. The mechanism of glucose oxidation at the DLC:N/Au electrodes was examined in detail.

## EXPERIMENTAL

### Reagents

D-Glucose (purity 98 %) and  $\text{HAuCl}_4\cdot 3\text{H}_2\text{O}$  (purity 99.99 %) were supplied by Sigma, USA; deionized water was obtained from a Millipore Q purification system (resistivity  $>18 \text{ M}\Omega\text{cm}$ ); and 0.2 M buffer solutions with pH of 4, 7, and 10 were also supplied by Sigma, USA. All the chemicals were of analytical grade.

## Sample preparation

DLC:N thin films were deposited on conductive *n*-Si (100) substrates (0.001–0.0035  $\Omega\text{cm}$ ) via a filtered cathodic vacuum arc deposition process (Nanofilms) using a pure graphite target (99.95 % C) as the carbon source. When the pressure of the vacuum chamber was lowered to about  $2 \times 10^{-6}$  Torr, the Si substrates were etched by pure Ar plasma to remove surface oxide layers and impurities. During film deposition, 10-sccm nitrogen (99.999 %) was continuously introduced into the vacuum chamber and an arc was ignited by contacting the graphite anode against the graphite target (cathode), thus producing a mixed plasma of carbon and nitrogen passing through a double-bend off-plane filter and leading to a DLC:N film deposited on the substrate. All the depositions were carried out at a fixed-pulse voltage of 800 V. The DLC:N films with a thickness of about 100 nm were obtained by controlling the deposition time.

The as-prepared DLC:N films were anodically pretreated in a 0.1 M NaOH solution using an electrochemical workstation (CHI 660C) having a three-electrode cell consisting of DLC:N working electrode, Ag/AgCl (saturated KCl) reference electrode, and Pt foil counter electrode. The pretreatment potential was controlled in the range of  $-0.2$  to  $1.0$  V (vs. Ag/AgCl) until a stable current response was obtained after 10 cycles (Fig. 1). The NaOH-treated DLC:N films were then immersed into a 0.1 M  $\text{H}_2\text{SO}_4$  solution containing 0.1 mM  $\text{HAuCl}_4$  to electrodeposit Au NCs on the film surfaces. The deposition potential was controlled from  $0.9$  to  $-0.1$  V (vs. Ag/AgCl) for 1, 3, 5, and 8 cycles at a scan rate of  $0.02$  V/s under nitrogen bubbling conditions, and the DLC:N/Au samples prepared were correspondingly labeled as DLC:N/Au1 to DLC:N/Au8 with respect to increased cycles. The as-prepared DLC:N/Au electrodes were cycled in a 0.1 M  $\text{H}_2\text{SO}_4$  solution until stable voltammograms were achieved, indicating the complete cleaning of the Au active areas. The apparent geometric surface area of all the DLC:N and DLC:N/Au films was about  $0.1$   $\text{cm}^2$ .

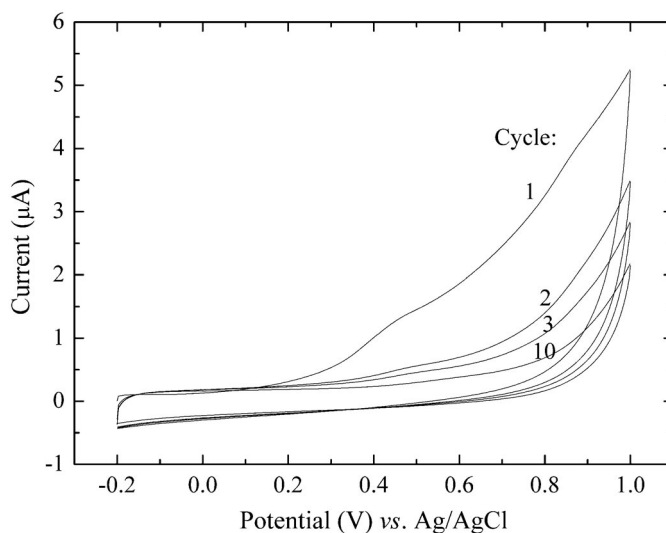


**Fig. 1** Cyclic voltammograms (CVs) of DLC:N electrodes in 0.1 M NaOH solution with a scan rate of 0.05 V/s.

## Electrode characterization

The composition and chemical bonding structure of DLC:N and DLC:N/Au films were measured by XPS (Kratos Axis Ultra) with Al  $\text{K}\alpha$  (1486.6 eV) as the X-ray source. XPS core level spectra for C 1s, N 1s, O 1s, and Au 4f were acquired at a 0.125 eV step with a pass energy of 40 eV. The composition of the DLC:N films was analyzed and quantified for N, C, and O elements from the total areas of the

XPS bands corresponding to the N 1s, C 1s, and O 1s spectra. Raman analysis was performed using a Renishaw RM1000 confocal micro-Raman spectroscope with a He–Ne laser source (632.8 nm). The recorded Raman wave numbers ranged from 800 to 2000  $\text{cm}^{-1}$ .

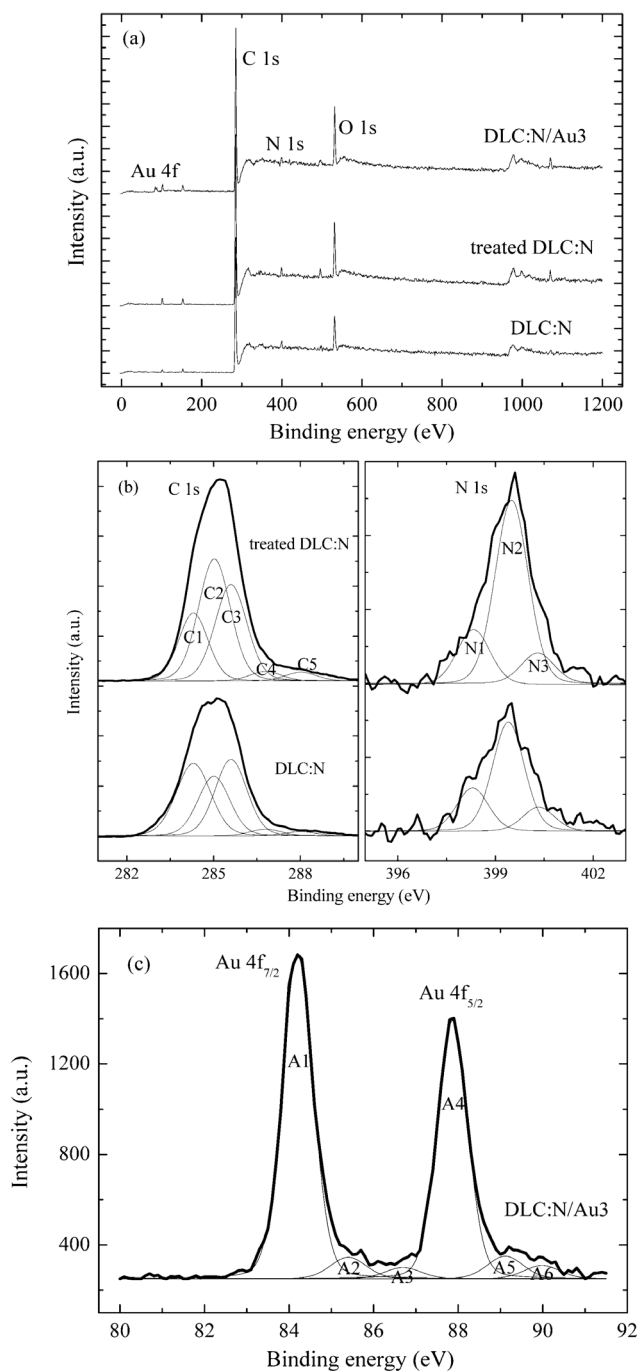
The deposition process of the Au NCs on the DLC:N films was analyzed by cyclic voltammetry in a 0.1 M  $\text{H}_2\text{SO}_4$  solution at different scan rates. The resulting Au NCs were examined using a Hitachi S4800 SEM. Voltammetric measurements for glucose oxidation at the DLC:N and DLC:N/Au electrodes were performed in buffer solutions with different pHs and 0.1 M NaOH solutions with and without glucose using the above three-electrode system. Electrochemical oxidation of glucose at a bulk Au electrode (0.1  $\text{cm}^2$ ) was also carried out for comparison. All the electrochemical experiments were carried out at 20 °C monitored by a thermostatic water jacket.

## RESULTS AND DISCUSSION

### Microstructures of DLC:N and DLC:N/Au films

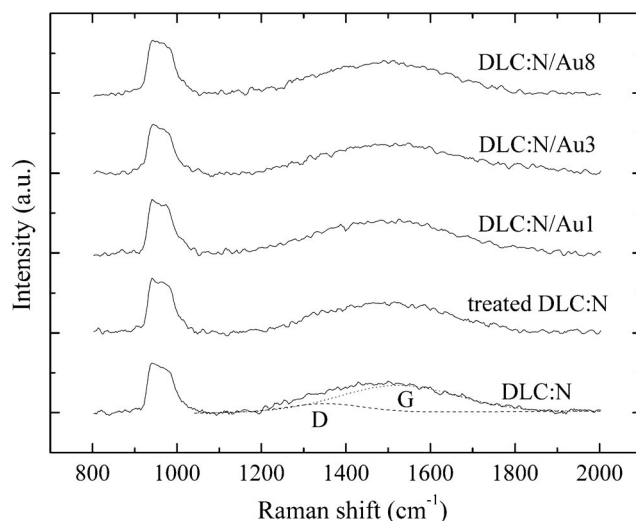
In previous reports, many physical or electrochemical methods including anodic, cathodic, and plasma treatments have been used to evolve the surface termination of BDD and active sites of amorphous carbon electrodes [23,33,34]. XPS measurement is effective to provide the surface information of different samples after surface treatment. The content of nitrogen in DLC:N film is calculated to be about 2.3 atom %. It can be seen from the XPS spectra of the as-prepared DLC:N, NaOH-treated DLC:N, and DLC:N/Au electrodes (Fig. 2a) that the oxygen signals for the NaOH-treated DLC:N electrode are enhanced after the NaOH treatment. The increase in oxygen content from about 7.3 to 9.4 atom % after the NaOH treatment indicates that the anodic pretreatment has promoted the oxygen-terminated surface. The adsorption of species involved in the oxygen evolution reaction occurs at more positive potentials (Fig. 1). Figure 2b shows the XPS core level spectra of C 1s and N 1s for the DLC:N before and after the NaOH treatment. The C1 ( $284.3 \pm 0.2$  eV) and C2 ( $285.0 \pm 0.2$  eV) peaks are attributed to C–C  $\text{sp}^2$ -coordinated bonds in graphite and C–C  $\text{sp}^3$  bonds in diamond, respectively [35]. The C3 ( $285.6 \pm 0.2$  eV) and C4 ( $286.8 \pm 0.2$  eV) peaks are related to C=N bonds and C–N bonds, respectively [36]. The C5 peak at  $288.0 \pm 0.2$  eV is attributed to C=O bonding. After the NaOH treatment, the C5 peak is more obvious, indicating the formation of oxygen-terminated surface. The N 1s core level spectra can be decomposed into three peaks at  $398.3 \pm 0.2$ ,  $399.4 \pm 0.2$ , and  $400.3 \pm 0.2$  eV. The N1 and N2 peaks are attributed to  $\text{sp}^3$  C–N and  $\text{sp}^2$  C=N bonds, respectively [37]. The N3 peak is related to the N–O bonding in the surface layer. It is clear that most of the N atoms are bonded to the  $\text{sp}^2$ -bonded carbon. The Au  $4f_{7/2}$  and Au  $4f_{5/2}$  peaks located at  $84.2 \pm 0.1$  and  $87.8 \pm 0.1$  eV for the Au NPs (Fig. 2c) are found to be higher than those for the Au foil ( $83.9 \pm 0.1$  and  $87.6 \pm 0.1$  eV). These small shifts in core-level binding energy can be attributed to a quantum size effect [38]. The Au 4f core-level spectrum can be characterized by three pairs of peaks: the peaks at  $84.2 \pm 0.1$  and  $87.9 \pm 0.1$  eV related to elemental gold ( $\text{Au}^0$ ), the peaks correlated with Au oxides of  $\text{Au}^+$  at  $85.4 \pm 0.1$  and  $89.1 \pm 0.1$  eV and of  $\text{Au}^{3+}$  at  $86.7 \pm 0.1$  and  $90.0 \pm 0.1$  eV. By integrating the relative peaks, their respective atomic percentages are estimated to be about 87.9 % for  $\text{Au}^0$ , 7.8 % for  $\text{Au}^+$ , and 4.3 % for  $\text{Au}^{3+}$ . The XPS results indicate that the surfaces of the Au NCs are partially oxidized to form Au oxides during the positive scans [39]. The Au oxides covering the surfaces of the Au NCs may be served as a mediator and provide an electrocatalytic activity together with the Au NCs.

Figure 3 shows the Raman spectra of the as-prepared DLC:N, NaOH-treated DLC:N, and DLC:N/Au electrodes. The peaks from 900 to 1040  $\text{cm}^{-1}$  are the second-order peaks of Si. The asymmetric broad peaks centered at about 1500  $\text{cm}^{-1}$  are determined as the first-order peaks of carbon, which are fitted by two Gaussian lines, i.e., D peak centered at about  $1350 \pm 2$   $\text{cm}^{-1}$  and G peak centered at  $1523 \pm 5$   $\text{cm}^{-1}$ . Generally, the G peak is attributed to the bond stretching of all pairs of  $\text{sp}^2$  atoms in aromatic rings as well as chains, while the D peak is related to the breathing modes of  $\text{sp}^2$  sites only in aromatic rings [40]. Neither significant differences in structure nor remarkable variations in the  $I_D/I_G$  ratio



**Fig. 2** XPS spectra of as-prepared DLC:N, NaOH-treated DLC:N, and DLC:N/Au3 electrodes: (a) full spectra, (b) C 1s and N 1s core level spectra, and (c) Au 4f core level spectrum.

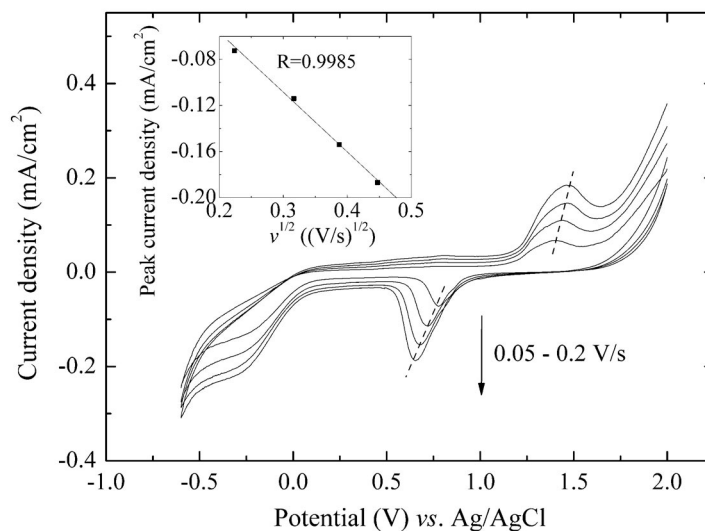
for the NaOH-treated DLC:N and DLC:N/Au electrodes are observed from the Raman spectra, which indicates that the anodic treatment and metal modification affect the surface termination of the DLC:N films but do not significantly modify the microstructure of the bulk DLC:N thin films.



**Fig. 3** Raman spectra of as-prepared DLC:N, NaOH-treated DLC:N, and DLC:N/Au electrodes. The DLC:N/Au electrodes were prepared after different deposition cycles in the 0.1 M  $\text{H}_2\text{SO}_4$  solution containing 0.1 mM  $\text{HAuCl}_4$ .

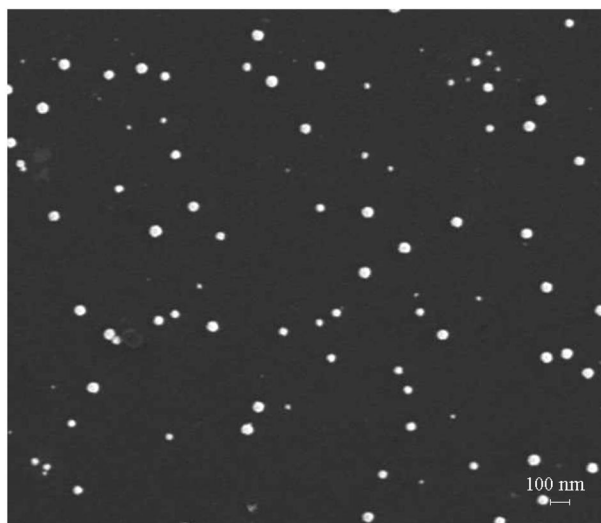
### Deposition process and morphology of Au NCs

Figure 4 illustrates the cyclic voltammograms (CVs) of the DLC:N/Au3 electrode in the 0.2 M  $\text{H}_2\text{SO}_4$  solution at different scan rates. Reduction peaks of Au are observed at about 0.77 V in the negative scans, and the peaks at about  $-0.21$  V are related to the reduction of hydrogen ions to hydrogen adatoms. The peaks at about 1.40 V in the positive curves are verified due to the oxidation of the deposited Au NCs on the DLC:N surfaces. Furthermore, the reduction and oxidation peaks of Au shift cathodically and anodically, respectively, with increasing sweep rate. A linear relationship between the reduction peak current density and the square root of scan rate (correlation coefficient,  $R = 0.9985$ ) indicates that the reduction process of Au is diffusion-controlled as shown in the inset in Fig. 4.



**Fig. 4** CVs of DLC:N/Au3 electrode in 0.2 M  $\text{H}_2\text{SO}_4$  solution with different scan rates. The inset shows the linear relation between cathode peak current density and square root of scan rate.

Figure 5 displays the SEM micrograph of DLC:N/Au<sub>3</sub> electrode surface on which the Au/AuO<sub>x</sub> NCs deposited after one cycle uniformly distribute, with the sizes ranging from 10.2 to 68.8 nm with a 35.6-nm mean value. Increasing the deposition time can enlarge the size of the Au/AuO<sub>x</sub> NCs. The mean diameters of the Au/AuO<sub>x</sub> NCs on the DLC:N/Au<sub>3</sub>, DLC:N/Au<sub>5</sub>, and DLC:N/Au<sub>8</sub> electrodes are about 40.3, 51.0, and 68.5 nm, respectively. The densities of the Au/AuO<sub>x</sub> NCs on the DLC:N/Au electrode surfaces are roughly calculated to be 10<sup>8</sup> to 10<sup>9</sup> clusters per cm<sup>2</sup>.



**Fig. 5** SEM micrograph of DLC:N/Au<sub>3</sub> electrode surface.

### Glucose detection on DLC:N and DLC:N/Au electrodes

#### *Voltammetric response and mechanism of glucose oxidation at DLC:N and DLC:N/Au electrodes in solutions with different pHs*

Figure 6 shows the CVs obtained at the NaOH-treated DLC:N electrode in the 0.1 M NaOH solutions (pH 14) without and with 5 mM glucose. No obvious response is observed at the NaOH-treated DLC:N electrode within the potential window, hinting at a low electrochemical activity of the DLC:N electrode for glucose oxidation. Comparatively, the DLC:N/Au<sub>3</sub> electrode represents an evident current response to glucose in the NaOH solution (Fig. 6b). The Au oxidation starts at about 0.25 V and peaks at around 0.5 V (peak A), and the Au reduction peak (peak B) is observed at about 0.17 V (dashed curve in Fig. 6b). When 5 mM glucose is added into the NaOH solution, the glucose oxidation begins at approximately -0.5 V during the positive potential scans and shows two distinctive peaks at about -0.14 V (peak C) and 0.37 V (peak D), respectively. The first band is speculated to correspond to the oxidation of the aldehyde functionality of glucose to produce the gluconate anions (gluconolactone or gluconate) in this alkaline medium, which is in agreement with the literature [41,42]. The second peak is speculated to correspond to the oxidation of the primary alcohol of the gluconate anions to produce gluconate dianions. As the potential is swept further positively, the rate of glucose oxidation decreases and the glucose oxidation virtually ceases at  $E > 0.5$  V due to the formation of trivalent Au oxides. During the negative sweep, an intense re-oxidation peak (peak E at about 0.16 V) appears in the same potential region as soon as the Au oxides are reduced. Increasing the scan rate moves peaks C and D to the positive direction. The linear relationships between the oxidation peak current densities,  $i_p$ , for peaks C and D and the scan rate,  $\nu$ , in a scale of logarithm are investigated ( $R = 0.9984$  for peak C and  $R = 0.9998$  for peak D). A  $(\partial \log i_p / \partial \log \nu)$  value of about 1.0 for peak C suggests a control by adsorp-

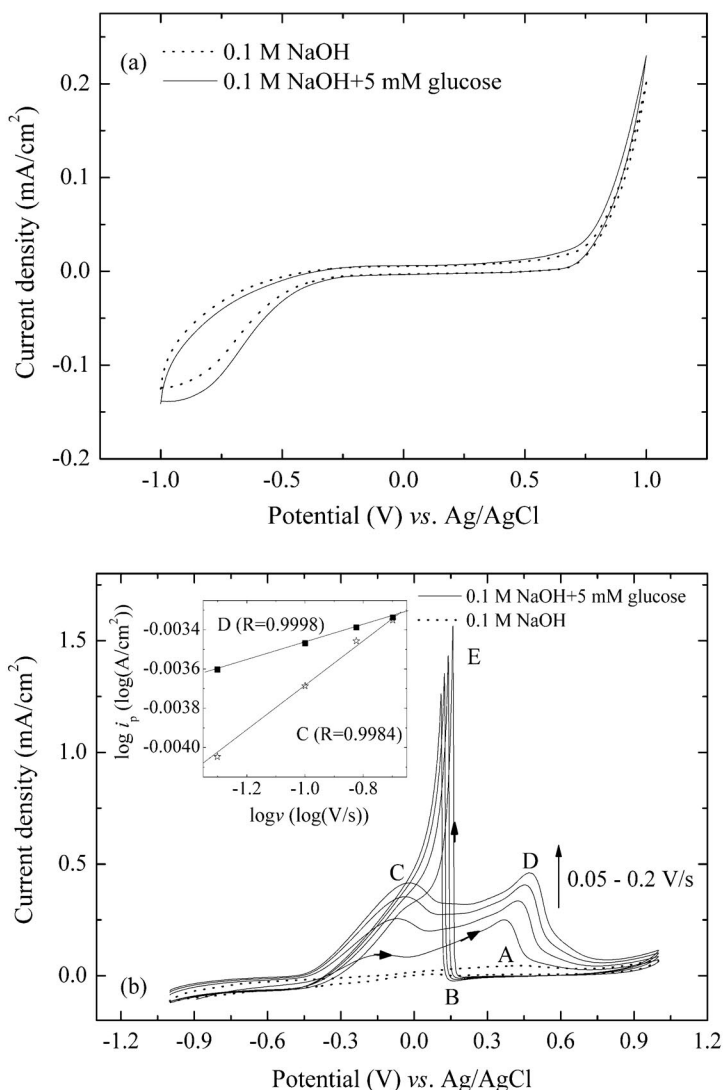


**Fig. 6** CVs obtained at (a) NaOH-treated DLC:N and (b) DLC:N/Au<sub>3</sub> electrodes in the 0.1 M NaOH solutions without or with 5 mM glucose. The inset in (b) shows the linear relations between oxidation peak current density of glucose and scan rate in logarithm.

tion for glucose oxidation while  $(\partial \log i_p / \partial \log v) = 0.45$  for peak D suggests a control by diffusion for glucose oxidation at the DLC:N/Au<sub>3</sub> electrode. The current densities of re-oxidation peak E decrease and the positions shift toward the negative direction with successive cycles and increased scan rates, which indicates the poisoning of the electrode surfaces. A reactivation program at 1.5 V for 1 s or cathodic desorption of carbohydrate residues at -1.0 V for 10 ms is effective to maintain the electrode activity [5,43].

No peaks related to glucose oxidation are observed from acidic (pH 4) and neutral (pH 7) systems. The glucose oxidation in an alkaline solution with pH 10 is weaker than that in a NaOH solution with pH 14. These results have been explained as the lack of formation of a catalytic hydrous Au oxide, i.e., AuOH<sub>ads</sub>, in acidic and neutral solutions [3,44] because the formation rate of AuOH<sub>ads</sub> is dependent upon the amount of OH<sup>-</sup> transported to the electrode surface. On the DLC:N/Au electrode surface,

the Au/AuOx NCs can act as a strong oxidant and directly react with the organic compounds by abstracting hydrogen atoms to yield radicals. The resulting radicals further react with additional surface sites to form some products. The possible reaction pathways are suggested as follows [5]. Firstly, a catalytic AuOH is formed in the solution. A glucose molecule then adsorbs onto the AuOH site, and the transfer of an electron from the adsorbed species to an Au site occurs to form gluconolactone.

#### Au size effect on response current of glucose oxidation

Furthermore, the DLC:N/Au electrodes with different sizes of Au NCs are used to oxidize the glucose. Figure 7 shows the CVs of the DLC:N/Au and bulk Au electrodes in the 0.1 M NaOH solutions without and with 1 mM glucose at a scan rate of 0.1 V/s. The current density of glucose oxidation depends

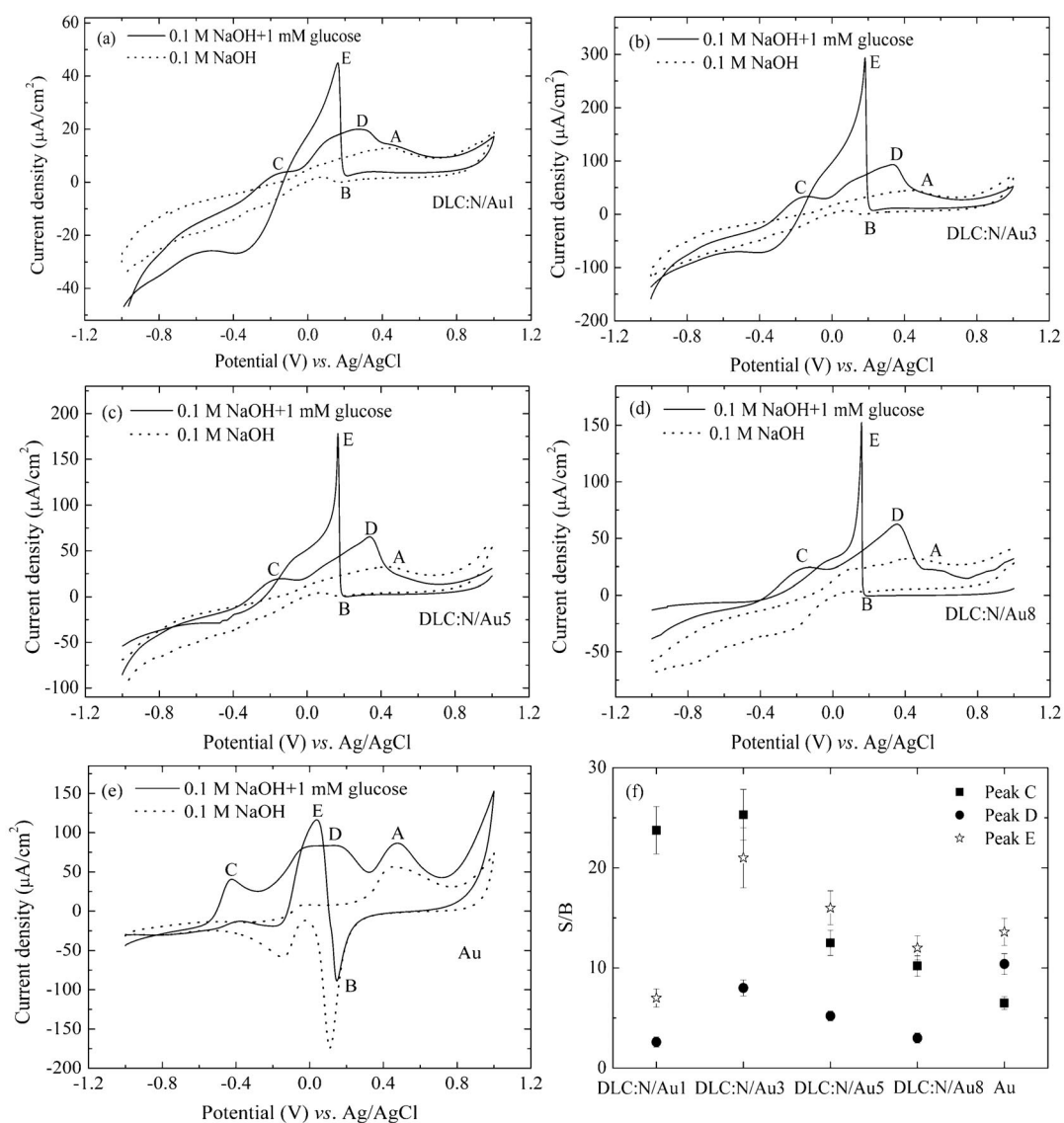
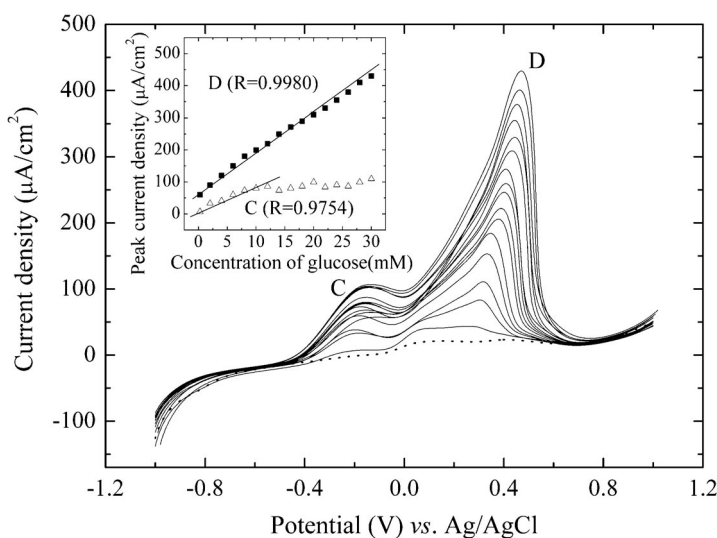


**Fig. 7** CVs of DLC:N/Au and bulk Au electrodes in the 0.1 M NaOH solutions without or with 1 mM glucose: (a) DLC:N/Au1, (b) DLC:N/Au3, (c) DLC:N/Au5, (d) DLC:N/Au8, and (e) bulk Au. (f) S/B ratios obtained from the current response of different electrodes in the 0.1 M NaOH solutions without or with 1 mM glucose.

on the size of Au NCs. When 35.6-nm Au NCs are deposited on a DLC:N electrode surface, the real surface area of the DLC:N electrode increases accompanied by the enhanced catalytical activity for glucose oxidation and signal/background (S/B) ratio. The Au NCs can be regarded as microelectrodes uniformly distributed on the DLC:N electrode surface and a higher detection current density can be obtained at each Au NC. Three-cycle deposition induces a higher current response due to an increase in average diameter of Au NCs (Fig. 7b). Further lengthening the deposition time improves the growth of the Au NCs but promotes the background current as well, resulting in the decreased S/B ratios (Figs. 7c,d,f). In a study, Hutton and co-workers reported that the exchange current density of platinum cluster-modified glassy carbon for hydrogen evolution increased with the decrease of Pt particle size [45]. Jia et al. also found that a biosensor fabricated with smaller Au NPs exhibited a larger response than that prepared with larger Au NPs [46]. The oxidation of glucose on the bulk Au electrode starts from about  $-0.55$  V and represents three oxidation characteristics in the positive (peak C at about  $-0.42$  V and plateau D from about  $-0.03$  to  $0.17$  V) and negative (peak E at about  $0.04$  V) scans (Fig. 7e). The current density obtained at the Au electrode decreases quickly with time due to the electrode surface poisoning. A maximum S/B ratio is obtained with the DLC:N/Au3 electrode, indicating that the catalytical ability of this electrode is the best among the DLC:N/Au electrodes used in this study. The DLC:N/Au3 electrode is therefore chosen for the following voltammetric measurements.

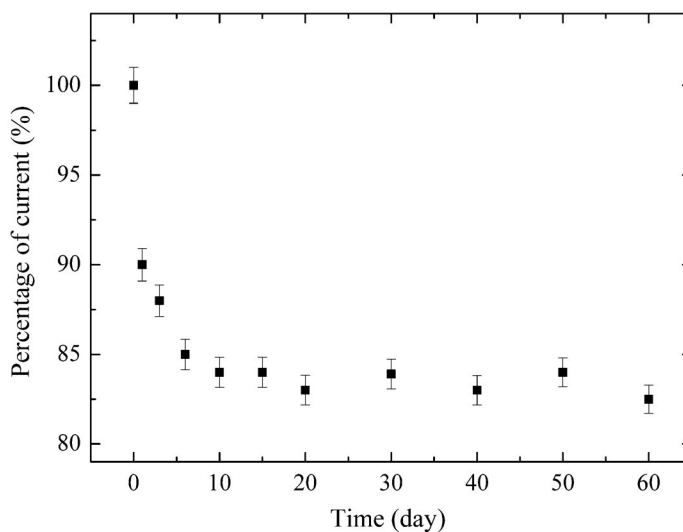
#### Linear calibration and repeatability of DLC:N/Au electrode

Figure 8 shows typical linear sweep voltammograms of glucose oxidation at the DLC:N/Au3 electrode with successive increments of glucose in concentration in the 0.1 M NaOH solution, and the linear characteristics of the electrode for glucose detection are investigated. The current density of peak C does not show a good linear characteristic with the increase of glucose concentration. This means that the oxidation process of glucose to form gluconolactone is controlled by adsorption. The current density of peak D is linear within a wide concentration range from 0.25 to 30 mM ( $R = 0.9980$ ) with a sensitivity of  $12.0 \pm 1.0$  A/(cm<sup>2</sup> mM). The detection limit, based on a signal-to-noise (S/N) ratio of 3, is estimated to be  $60 \pm 2$   $\mu$ M. This range is broader than the blood glucose level of a normal human body (4–7 mM). The linear glucose response based on the DLC:N/Au3 electrode is therefore enough and suitable for the practical application in determining blood sugar concentration.



**Fig. 8** Linear sweep voltammograms of DLC:N/Au3 electrode with respect to increase in glucose concentrations in 0.1 M NaOH solutions. The inset shows the relation between the oxidation current density and concentration of glucose obtained at DLC:N/Au3 electrode in the 0.1 M NaOH solutions.

The repeatability of the DLC:N/Au<sub>3</sub> electrode is tested as shown in Fig. 9 where the relative standard deviation of amperometric current responses recorded by 20 injections of 1 mM glucose in the 0.1 M NaOH solutions is calculated to be about 5.7 %. The stability of the DLC:N/Au<sub>3</sub> electrode is investigated over a 60-day period. The glucose oxidation current exhibits a sharp drop to about 83 % of the initial response after 2 weeks due to the absence of some Au NCs. However, the current response of the electrode remains relatively stable throughout the rest of the 60-day period, implying a long-term stability of the electrode.



**Fig. 9** Long-term stability of DLC:N/Au<sub>3</sub> electrode in the 0.1 M NaOH solution with 1 mM glucose over a 60-day period.

## CONCLUSIONS

DLC:N/Au thin film electrodes were fabricated by a filtered cathodic vacuum arc process followed by electrodeposition. An O-terminal surface was developed after the DLC:N thin films were treated by a NaOH solution. The size of the Au NCs covered by a Au oxide layer could be adjusted by controlling the electrodeposition time. The Au/AuO<sub>x</sub> NCs significantly improved the electrochemical activity of DLC:N electrodes toward glucose oxidation due to the catalytic actions of AuOH<sub>ads</sub> species in the alkaline solutions. A maximum S/B ratio of glucose oxidation was obtained with the DLC:N/Au electrodes with smaller Au NCs. The glucose oxidation at about -0.1 and 0.4 V was controlled by adsorption and diffusion processes, respectively. A wide detection range of glucose concentrations from about 0.25 to 30 mM, and a low detection limit of about 60 μM were obtained with the DLC:N/Au electrodes, which implies that the DLC:N/Au electrodes developed in this study may further be applied as a non-enzymatic glucose biosensor due to their instant response, high sensitivity, and good reproducibility.

## ACKNOWLEDGMENTS

This work was supported by the Environment and Water Industry Development Council (EWI) of Singapore (Project No. 0601-IRIS-035-00), the National Natural Science Foundation of China (Grant No. 50902123), and the Scientific Research Fund of Zhejiang Provincial Education Department (Grant No. Y200806012).

## REFERENCES

1. K. Borch-Johnsen, A. Neil, B. Balkau, S. Larsen, K. Borch-Johnsen, A. Nissinen, J. Pekkanen, J. Tuomilehto, S. Keinanen-Kiukaanniemi, L. Hiltunen, S. L. Kivela, J. Tuomilehto, P. Jousilahti, J. Lindstrom, M. Pyorala, K. Pyorala, B. Balkau, E. Eschwege, G. Gallus, M. P. Garancini, A. Schranz, R. J. Heine, J. M. Dekker, E. Feskens, H. Lithell, B. Zethelius, M. Peltonen, N. Unwin, N. Ahmad, K. G. M. M. Alberti, M. M. Alberti, K. Borch-Johnsen, J. Eriksson, Q. Qiao, J. Tuomilehto, Q. Qiao, B. Balkau, J. Tuomilehto, Q. Qiao, K. Borch-Johnsen, B. Balkau. *Lancet* **354**, 617 (1999).
2. J. W. Lee, J. D. Helmann. *Diabetes Care* **23**, 208 (2000).
3. L. A. Larew, D. C. Johnson. *J. Electroanal. Chem.* **262**, 167 (1989).
4. H. W. Lei, B. L. Wu, C. S. Cha, H. Kita. *J. Electroanal. Chem.* **382**, 103 (1995).
5. P. Parpot, S. G. Pires, A. P. Bettencourt. *J. Electroanal. Chem.* **566**, 401 (2004).
6. S. Ben Aoun, Z. Dursun, T. Koga, G. S. Bang, T. Sotomura, I. Taniguchi. *J. Electroanal. Chem.* **567**, 175 (2004).
7. S. Gilman. In *Electroanalytical Chemistry*, A. J. Bard (Ed.), pp. 111–192, Marcel Dekker, New York (1967).
8. R. G. Compton, J. S. Foord, F. Marken. *Electroanalysis* **15**, 1349 (2003).
9. R. L. McCreery. *Chem. Rev.* **108**, 2646 (2008).
10. T. Tatsuma, H. Mori, A. Fujishima. *Anal. Chem.* **72**, 2919 (2000).
11. R. Maalouf, H. Chebib, Y. Saikali, O. Vittori, M. Sigaud, F. Garrelie, C. Donnet, N. Jaffrezic-Renault. *Talanta* **72**, 310 (2007).
12. H. Cachet, C. Deslouis, M. Chouiki, B. Saidani, N. M. J. Conway, C. Godet. *J. Electrochem. Soc.* **149**, E233 (2002).
13. J. Robertson. *Mater. Sci. Eng. R* **37**, 129 (2002).
14. Z. E. Zhang, H. Y. Liu, J. Q. Deng. *Anal. Chem.* **68**, 1632 (1996).
15. J. Wang, J. A. Carlisle. *Diamond Relat. Mater.* **15**, 279 (2006).
16. Y. Liu, M. K. Wang, F. Zhao, Z. A. Xu, S. J. Dong. *Biosens. Bioelectron.* **21**, 984 (2005).
17. Y. H. Lin, F. Lu, Y. Tu, Z. F. Ren. *Nano. Lett.* **4**, 191 (2004).
18. S. Q. Liu, H. X. Ju. *Biosens. Bioelectron.* **19**, 177 (2003).
19. S. Park, H. Boo, T. D. Chung. *Anal. Chim. Acta* **556**, 46 (2006).
20. J. S. Ye, Y. Wen, W. D. Zhang, L. M. Gan, G. Q. Xu, F. S. Sheu. *Electrochem. Commun.* **6**, 66 (2004).
21. A. Lagrini, C. Deslouis, H. Cachet, M. Benlahsen, S. Charvet. *Electrochem. Commun.* **6**, 245 (2004).
22. K. Yoo, B. Miller, X. Shi, R. Kalish. *J. Electrochem. Soc.* **148**, C95 (2001).
23. A. P. Liu, J. Q. Zhu, J. C. Han, H. P. Wu, W. Gao. *Electroanalysis* **19**, 1773 (2007).
24. G. C. Yang, E. J. Liu, N. W. Khun, S. P. Jiang. *J. Electroanal. Chem.* **627**, 51 (2009).
25. M. C. Daniel, D. Astruc. *Chem. Rev.* **104**, 293 (2004).
26. G. J. Hutchings. *Catal. Today* **100**, 55 (2005).
27. B. Hvolbæk, T. V. W. Janssens, B. S. Clausen, H. Falsig, C. H. Christensen, J. K. Nørskov. *Nano Today* **2**, 14 (2007).
28. T. Watanabe, T. A. Ivandini, Y. Makide, A. Fujishima, Y. Einaga. *Anal. Chem.* **78**, 7857 (2006).
29. M. L. Mena, P. Yanez-Sedeno, J. M. Pingarron. *Anal. Biochem.* **336**, 20 (2005).
30. S. Hrapovic, Y. L. Liu, K. B. Male, J. H. T. Luong. *Anal. Chem.* **76**, 1083 (2004).
31. K. B. Male, S. Hrapovic, Y. L. Liu, D. S. Wang, J. H. T. Luong. *Anal. Chim. Acta* **516**, 35 (2004).
32. A. Salimi, E. Sharifi, A. Noorbakhsh, S. Soltanian. *Biosens. Bioelectron.* **22**, 3146 (2007).
33. M. Benlahsen, H. Cachet, S. Charvet, C. Debiemme-Chouvy, C. Deslouis, A. Lagrini, V. Vivier. *Electrochem. Commun.* **7**, 496 (2005).

34. G. R. Salazar-Banda, L. S. Andrade, P. A. P. Nascente, P. S. Pizani, R. C. Rocha, L. A. Avaca. *Electrochim. Acta* **51**, 4612 (2006).
35. Z. Wang, C. B. Wang, Q. Wang, J. Y. Zhang. *J. Appl. Phys.* **104**, 073306 (2008).
36. J. J. Li, W. T. Zheng, Z. S. Jin, T. X. Gai, G. R. Gu, H. J. Bian, C. Q. Hu. *Vacuum* **72**, 233 (2004).
37. R. McCann, S. S. Roy, P. Papakonstantinou, M. F. Bain, H. S. Gamble, J. A. McLaughlin. *Thin Solid Films* **482**, 34 (2005).
38. H. G. Boyen, A. Ethirajan, G. Kastle, F. Weigl, P. Ziemann, G. Schmid, M. G. Garnier, M. Buttner, P. Oelhafen. *Phys. Rev. Lett.* **94**, 016804 (2005).
39. J. P. Sylvestre, S. Poulin, A. V. Kabashin, E. Sacher, M. Meunier, J. H. T. Luong. *J. Phys. Chem. B* **108**, 16864 (2004).
40. A. C. Ferrari, J. Robertson. *Phys. Rev. B* **61**, 14095 (2000).
41. E. M. Belgsir, E. Bouhier, H. Essis Yei, K. B. Kokoh, B. Beden, H. Huser, J. M. Leger, C. Lamy. *Electrochim. Acta* **36**, 1157 (1991).
42. M. Tominaga, T. Shimazoe, M. Nagashima, I. Taniguchi. *Electrochem. Commun.* **7**, 189 (2005).
43. M. B. Jensen, D. C. Johnson. *Anal. Chem.* **69**, 1776 (1997).
44. P. Ocon, C. Alonso, R. Celdran, J. Gonzalez-Velasco. *J. Electroanal. Chem.* **206**, 179 (1986).
45. H. D. Hutton, N. L. Pocard, D. C. Alsmeyer, O. J. A. Schueller, R. J. Spontak, M. E. Huston, W. H. Huang, R. L. McCreery, T. X. Neenan, M. R. Callstrom. *Chem. Mater.* **5**, 1727 (1993).
46. J. B. Jia, B. Q. Wang, A. G. Wu, G. J. Cheng, Z. Li, S. J. Dong. *Anal. Chem.* **74**, 2217 (2002).